https://doi.org/10.5194/essd-2026-575
Preprint. Discussion started: 2 November 2026
© Author(s) 2026. CC BY 4.0 License.



Open Access Earth System Science Data Discussions

A global inventory of rock glaciers

Jinhao Xu[1], Min Feng[1,2], Yanan Su[1], Dezhao Yan[3], Qinglin Wu[1,2], Peng Zhao[4], Xuefei Zhang[5], Xin Li[1]

[1]National Tibetan Plateau Data Center, State Key Laboratory of Tibetan Plateau Earth System, Environment and Resources, Institute of Tibetan Plateau Research, Chinese Academy of Sciences, Beijing 100101, China

[2]University of Chinese Academy of Sciences, Beijing 100049, China

[3]School of Water Resources and Environment, Hebei GEO University, Shijiazhuang 050031, China

[4]Shaanxi Zhongcheng Planning and Design Research Institute Co., Ltd, Xi'an 710000, China

[5]Land Satellite Remote Sensing Application Center, Ministry of Natural Resources, Beijing 100048, China

Correspondence to: Min Feng (mfeng@itpcas.ac.cn)

Abstract

Rock glaciers are among the most widespread visible expressions of ice-rich mountain permafrost. Although the significance of rock glaciers is relatively well understood at regional scales, differences among existing inventories in source data, interpretation criteria, mapping methods, and mapping scales hinder assessment of global rock glacier extent and distribution. Here we present the first rock glacier inventory built under a single, globally consistent mapping framework, produced by applying an ensemble of semantic-segmentation models to high-resolution (~2.4 m) satellite imagery, followed by expert manual post-processing and independent visual assessment. At 301 524 mapped polygons covering 38 849 km^2 across 19 major mountain and high-latitude regions worldwide, this is, to our knowledge, the most spatially extensive rock glacier

https://doi.org/10.5194/essd-2026-575
Preprint. Discussion started: 2 November 2026
© Author(s) 2026. CC BY 4.0 License.

inventory compiled to date, with standardized topographic, climatic, and permafrost-related attributes attached to every polygon. Independent visual assessment of 3015 polygons yielded a feature-level precision of 90.9 % against the adopted morphological identification criteria, supporting the dataset's use as a global occurrence baseline. Mapped rock glaciers are strongly concentrated in a small number of major mountain systems and follow a coherent elevation-latitude structure worldwide, extending from low elevations in high-latitude mountains to above 4000 m in low- and mid-latitude ranges, with larger mapped areas on moderate slopes and poleward-facing aspects associated with cold to near-freezing modeled ground temperatures. Approximately 91.8 % of the mapped area coincides with independently modeled permafrost-potential terrain, providing a consistency check against modeled permafrost conditions. The polygon boundaries mapped under common criteria and standardized environmental attributes enable cross-regional comparison, support evaluation of mountain permafrost indicators, provide a spatial basis for prioritizing field and kinematic observations, and help identify mountain systems where hidden ice, long-term water storage, and permafrost-related geomorphic activity may require closer attention in a warming climate. The dataset is publicly available at https://doi.org/10.11888/Cryos.tpdc.303562 (Xu et al., 2026).

1 Introduction

Periglacial environments are among the natural systems most sensitive to climate change, and their evolution responds to variations in temperature and permafrost conditions in high-mountain regions (French, 2017). Among the landforms developed in these environments, rock glaciers are especially important because they provide a surface expression of ice-rich mountain permafrost and are closely associated with sediment transfer, slope evolution, and mountain hydrological processes (Ballantyne, 2001). Rock glaciers are debris landforms formed by past or ongoing permafrost creep.

https://doi.org/10.5194/essd-2026-575
Preprint. Discussion started: 2 November 2026
© Author(s) 2026. CC BY 4.0 License.



Open Access Earth System Science Data Discussions

Frontal and lateral margins constitute their defining morphological features and typically form steep slopes. Compression and differential movement during creep can produce transverse or longitudinal ridges and furrows on rock glacier surfaces (RGIK, 2023; Brardinoni et al., 2026).

The formation of rock glaciers depends strongly on ice-rich permafrost conditions, and their spatial distribution provides geomorphological evidence of present and past mountain permafrost (Barsch, 1996; Li, 2024; Brardinoni et al., 2026). At regional scales, rock glaciers are commonly used to constrain and validate permafrost distribution models and to support the development of permafrost probability maps and index-based products (Remya et al., 2024; Hu et al., 2024; Yan et al., 2025). Rock glaciers possess both solid and liquid water storage capacity (Harrington et al., 2018; Wagner et al., 2021) and are considered a potential long-term water resource (D. B. Jones et al., 2018), particularly in arid and semi-arid regions (Rangecroft et al., 2015). In addition, compared with glacier meltwater and groundwater, meltwater derived from rock glaciers exhibits distinct physical and chemical characteristics as well as pronounced seasonal variability (Brighenti et al., 2019; Schaffer et al., 2019). The motion of rock glaciers responds rapidly to changes in the thermal and hydrological conditions of permafrost (Lambiel and Delaloye, 2004; Haeberli et al., 2006; Knight, 2019). In recent decades, rock glacier velocities in many regions worldwide have been found to exhibit pronounced short-term variability and long-term trends, including acceleration and deceleration (Hartl et al., 2016; Eriksen et al., 2018; Kääb et al., 2021; Manchado et al., 2024). Such observable kinematic responses make rock glacier motion an important dynamic indicator of permafrost responses to climate change, and rock glacier velocity has been incorporated into global climate observation frameworks as a parameter for monitoring permafrost (Zemp et al., 2022; Brardinoni et al., 2026). Accelerated movement or structural destabilization of rock glaciers may further induce slope failures and trigger hazards such as rockfalls, debris flows, and lake outburst floods (Roer et al., 2008; Kofler et al., 2021), posing potential threats to downstream

https://doi.org/10.5194/essd-2026-575
Preprint. Discussion started: 2 November 2026
© Author(s) 2026. CC BY 4.0 License.



infrastructure and human activities (Lugon and Stoffel, 2010; Blöthe et al., 2019). Moreover, owing to the insulating debris cover and internal ventilation processes, rock glaciers can persist in the landscape after the retreat of nearby glaciers and snowfields, thereby providing longer-lasting cold habitats that may serve as important climate refugia for mountain biodiversity (Brighenti et al., 2021; Martini et al., 2024).

The absence of a globally harmonized inventory has made it difficult to assess the global distribution of rock glaciers (D. B. Jones et al., 2018; Brardinoni et al., 2019). Mountain permafrost is spatially heterogeneous and difficult to constrain globally from sparse ground observations, models, or indirect indicators alone; a harmonized rock glacier inventory can therefore provide a consistent observational layer for one of the few remotely identifiable geomorphic expressions of ice-rich mountain permafrost (Gruber, 2012; RGIK, 2023). Such an inventory would identify the mountain systems in which rock glaciers are concentrated, characterize their environmental settings, and help assess whether relationships identified in regional studies hold across a wider range of mountain environments (Haeberli et al., 2006; Zemp et al., 2022). As clean glacier ice retreats, debris-covered and permafrost landforms may become increasingly important expressions of frozen water and permafrost-related geomorphic activity in mountain landscapes (Brighenti et al., 2024; Haeberli et al., 2024). A global inventory would therefore provide a spatial basis for assessing the distribution, concentration, and topoclimatic settings of rock glaciers across these changing mountain systems.

Regional rock glacier mapping has accelerated with high-resolution optical imagery and InSAR-based Earth observation, making it possible to detect and characterize rock glaciers across individual mountain systems (Zhang et al., 2021; Hassan et al., 2024). Inventories now exist for several major rock glacier regions worldwide, including the European Alps (Krainer and Ribis, 2012), the Tibetan Plateau (Feng et al., 2025), the Peruvian Andes (Medina et al., 2026), the contiguous United States (Johnson et al., 2021), and northeastern Yakutia (Lytkin, 2020). These regional inventories have been essential for documenting abundance, activity, and relationships with mountain

https://doi.org/10.5194/essd-2026-575
Preprint. Discussion started: 2 November 2026
© Author(s) 2026. CC BY 4.0 License.



permafrost conditions within individual mountain systems (Boeckli et al., 2012; Hassan et al., 2021). Existing inventories also differ in survey footprint, image source, interpretation criteria, minimum mapping unit, treatment of compound landforms, and boundary placement, so direct combination of reported numbers, areas, and environmental distributions would introduce methodological bias (Brardinoni et al., 2019; Haeberli et al., 2024). The Rock Glacier Inventories and Kinematics (RGIK) framework provides a common geomorphological basis for comparing and integrating regional inventories (RGIK, 2023). Common inventorying criteria have been applied across diverse mountain environments, and collective review of individual interpretations helps reconcile differences in rock glacier identification and delineation (Rouyet et al., 2025). Combining geomorphological inventories with kinematic observations can advance understanding of creeping permafrost across mountain environments. Shared data structures further underpin the development of a global rock glacier database that can be updated and reused (Brardinoni et al., 2026). Gaps in inventory coverage persist in circum-Arctic high-latitude mountains, the West Asian highlands, southern Siberian mountain regions, and the Atlas Mountains. These gaps constrain global estimates of rock glacier extent and associated ice and water storage potential, as well as assessments of mountain permafrost and geomorphic activity (D. B. Jones et al., 2018; Brardinoni et al., 2019).

Producing this global spatial baseline requires scalable mapping, consistent geomorphological criteria, and comparable environmental attributes. The large volume of imagery and diversity of mountain environments make manual interpretation difficult to apply consistently at this scale. In recent years, deep learning-based approaches for automated remote sensing interpretation have provided new pathways for large-scale rock glacier identification and inventorying (Erharter et al., 2022; Hu et al., 2023). Recent studies have demonstrated that deep learning-based semantic segmentation models can detect rock glacier features at regional and cross-regional scales, improving mapping efficiency and supporting more consistent candidate

https://doi.org/10.5194/essd-2026-575
Preprint. Discussion started: 2 November 2026
© Author(s) 2026. CC BY 4.0 License.


generation (Sun et al., 2024; Feng et al., 2025). The performance of these methods is closely linked to the interpretability of landform features in imagery and the quality of manually compiled training datasets (Brardinoni et al., 2026). Cross-regional transferability also depends on how well training datasets represent the diversity of rock glacier morphologies and mountain environments (Rouyet et al., 2025). These advances make it possible to combine automated candidate generation with expert post-processing and independent validation, thereby supporting a scalable and geomorphologically constrained global inventory.

This study constructs a global rock glacier inventory under a unified framework for data preparation, interpretation criteria, mapping methods, and scale selection. The framework combines deep learning-assisted identification, manual post-processing, and independent assessment of inventory quality. The polygon boundaries and standardized environmental attributes provide a common observational basis for comparing rock glacier distribution among mountain systems, evaluating rock glaciers as indicators of mountain permafrost, and identifying regions where subsurface ice, long-term water storage, and permafrost-related geomorphic activity may warrant closer investigation.

2 Data

2.1 High-resolution satellite imagery

High-resolution satellite imagery was used as the primary data source for deep learning model training and large-scale rock glacier identification. The imagery was mainly obtained from ESRI World Imagery, with Google Satellite imagery used as a complementary source in areas where ESRI imagery was unavailable or incomplete. Together, these datasets provide near-global coverage of high-resolution satellite imagery suitable for visual interpretation of surface geomorphology.

https://doi.org/10.5194/essd-2026-575
Preprint. Discussion started: 2 November 2026
© Author(s) 2026. CC BY 4.0 License.


The satellite imagery used in this study generally has meter-scale or sub-meter native spatial resolution and was processed at a common working resolution of 2.4 m, allowing interpretation of characteristic rock glacier surface features such as frontal slopes, lateral margins, and ridge-and-furrow morphology. The input images were true-colour composites of the red, green, and blue visible bands, providing surface texture and landform morphology for interpretation.

The exact acquisition dates of the imagery are not consistently available, as both ESRI World Imagery and Google Satellite imagery are mosaicked products compiled from multiple sensors and acquisition periods. Rock glacier morphology can remain recognizable over decadal timescales despite measurable kinematic or volumetric changes (Eriksen et al., 2018; Manchado et al., 2024). Acquisition season and date can affect snow cover, feature visibility, and boundary interpretation. The inventory therefore combines observations from different acquisition periods.

2.2 Rock glacier inventories used for model training

Supervised model training requires rock glacier samples with reliable boundaries and consistent geomorphological representation. Training data were compiled from previously published, peer-reviewed rock glacier inventories and supplemented by manual delineation in Alaska and the Chukchi Peninsula, where no suitable public vector inventories were available (Table 1). The selection was guided by data availability, inventory quality, regional representativeness, and the need to include rock glaciers from different climatic, topographic, and geomorphological settings while maintaining as even a spatial distribution as practical.

https://doi.org/10.5194/essd-2026-575
Preprint. Discussion started: 2 November 2026
© Author(s) 2026. CC BY 4.0 License.



185 Table 1. Rock glacier records used for model training.

Region	No. of polygons	Total area	Source
Alaska	197	31 km^2	manual interpretation
Chukchi Peninsula	66	4 km^2	manual interpretation
Argentine Andes	1643	158 km^2	(IANIGLA, 2018)
eastern European Alps	278	18 km^2	(Kellerer-Pirklbauer et al., 2012)
Greater Caucasus	417	44 km^2	(Tielidze et al., 2023)
northern Norway	192	43 km^2	(Rouyet et al., 2021)
Tibetan Plateau	8420	1078 km^2	(Feng et al., 2025)
northern Tien Shan	198	33 km^2	(Wang et al., 2017)
contiguous United States	361	42 km^2	(Johnson et al., 2021)
northeastern Yakutia	266	18 km^2	(Lytkin, 2020)

For each inventory, selected representative subregions were used for training. Subregions were chosen through visual inspection and expert assessment to include representative rock glacier morphologies, avoid areas with persistent snow, cloud, shadow, or poor image quality, and reduce spatial clustering of samples within a single 190 mountain belt. This strategy allowed detailed manual checking and internal harmonization while keeping the training set manageable. A large proportion of the training polygons originates from the Tibetan Plateau because this region contains abundant and morphologically diverse rock glaciers (Feng et al., 2025), but additional regions were included to broaden environmental and geographic coverage. All training 195 polygons were visually re-evaluated using high-resolution satellite imagery; boundaries were adjusted where necessary, uncertain features were excluded, and additional features meeting the adopted morphological criteria within the selected areas were manually delineated.

Visual interpretation of training samples was based primarily on high-resolution true-200 colour satellite imagery, considering surface relief, texture and overall morphology together with the spatial relationship between the landform and its upslope debris source.

https://doi.org/10.5194/essd-2026-575
Preprint. Discussion started: 2 November 2026
© Author(s) 2026. CC BY 4.0 License.



Terrain data and topographic shadows in the imagery were used where needed to help interpret surface relief, slope changes and overall landform outlines. Transverse or longitudinal ridges and furrows, local surface undulations, and differences in texture and colour relative to adjacent talus slopes were examined together with a downslope-extending tongue-shaped or lobate form, a frontal slope and lateral margins. Where ridges and furrows were weakly developed, identification considered the spatial distribution of other surface-texture contrasts and their correspondence with the overall landform outline. Exposed ice, ice cliffs, supraglacial ponds, drainage channels and thermokarst depressions, which are more characteristic of debris-covered glaciers, were considered alongside these morphological features when interpreting debris-covered landforms. Where vegetation obscured surface texture, identification drew on the geomorphological setting, overall outline and discernible frontal and lateral features. Morphologically subdued landforms can have gentler marginal slopes and lower surface relief (RGIK, 2023; Brardinoni et al., 2026).

Training samples were delineated using extended geomorphological footprints that explicitly include frontal and lateral margins, following the recommendations of the Rock Glacier Inventories and Kinematics (RGIK) guidelines (RGIK, 2023; Brardinoni et al., 2026). Delineation followed the overall outline, using changes in the curvature of the frontal and lateral outlines, breaks in slope and contacts with the surrounding terrain. The front was identified from its terminal slope and upper and lower edges, and the lateral margins were traced along lateral slopes, levees or marginal furrows. Local changes in texture, colour and vegetation cover helped locate landform contacts. For talus-connected landforms, the upper boundary followed the concave transition at the talus base, informed by changes in slope and texture between the talus and the rock glacier below. Where the front was continuous with the rock glacier body and its outer boundary was clearly identifiable, the outline followed its contact with the surrounding terrain. For disrupted or discontinuous fronts with an indistinct lower boundary, an approximate horizontal distance of 50 m from the upper front edge was used as a

https://doi.org/10.5194/essd-2026-575
Preprint. Discussion started: 2 November 2026
© Author(s) 2026. CC BY 4.0 License.



reference for training-sample delineation. After quality control and harmonization, 12 038 rock glacier polygons were retained and used as positive samples for model training.

2.3 Topoclimatic datasets

To quantify the spatial distribution patterns of rock glaciers and to characterize their relationships with major topographic and climatic conditions, several globally consistent environmental datasets were used as auxiliary layers for descriptive and interpretative analyses.

Topographic information was derived primarily from the Forest and Buildings removed Copernicus DEM (FABDEM, Hawker et al., 2022), which provides a global digital elevation model with vegetation and building artefacts removed at 30 m spatial resolution. In the limited region where FABDEM coverage was incomplete, namely the Greater Caucasus, elevation data were supplemented using the NASA Digital Elevation Model (NASADEM, NASA JPL, 2020) to fill the gap in elevation coverage. Slope and aspect were derived from the DEM and included as topographic variables in the workflow and released attribute table.

Climatic conditions were characterized using the CHELSA v2.1 high-resolution climatology dataset (Karger et al., 2017). Long-term multi-year mean air temperature and precipitation were obtained from the CHELSA v2.1 climatological normals for the 1981–2010 reference period, provided at a spatial resolution of 30 arc-seconds. CHELSA v2.1 incorporates orographic effects and is widely used in mountainous and cryospheric studies, making it suitable for large-scale analyses of rock glacier distribution across diverse environmental settings.

Ground thermal conditions were represented using the UiO PEX–MAGT v5.0 global mean annual ground temperature (MAGT) dataset (Obu et al., 2018, 2019a, b), which provides modeled multi-year mean estimates of near-surface ground temperature at a spatial resolution of 1 km. The dataset represents multi-year mean conditions for the period 2000–2016, with 2000–2017 used for Antarctica. This dataset was employed to

https://doi.org/10.5194/essd-2026-575
Preprint. Discussion started: 2 November 2026
© Author(s) 2026. CC BY 4.0 License.


characterize the thermal environment associated with rock glacier occurrence and to support analyses of their relationship with permafrost conditions.

In addition, the Global Permafrost Zonation Index (PZI) map was used as an independent reference layer to describe large-scale permafrost zonation (Gruber, 2012). The PZI is based on long-term mean annual air temperature (MAAT) for the 1961–1990 reference period and is provided at a spatial resolution of 30 arc-seconds. It was used to facilitate the interpretation of rock glacier distribution in relation to broad permafrost zones.

2.4 Released dataset structure and metadata

The global rock glacier inventory is released as a polygon-based dataset with an associated attribute table, metadata, and validation information. The polygon layer is distributed as a GeoPackage in WGS 84 geographic coordinates (EPSG:4326), with each record linked to a stable feature identifier.

The final dataset includes polygon area, centroid coordinates, elevation, slope, aspect, mean annual air temperature, mean annual ground temperature, precipitation, and PZI attributes. Field definitions, units, coordinate reference information, no-data values, and processing provenance are documented in the product guide.

3 Methodology

We developed a deep-learning-based approach to identify rock glaciers and generate candidate polygons at a global scale. The overall workflow, illustrated in Fig. 1, follows a structured pipeline comprising study-area delineation, data preparation from satellite imagery, topographic data, and published inventories, model training and inferencing, and manual post-processing and validation.

https://doi.org/10.5194/essd-2026-575
Preprint. Discussion started: 2 November 2026
© Author(s) 2026. CC BY 4.0 License.



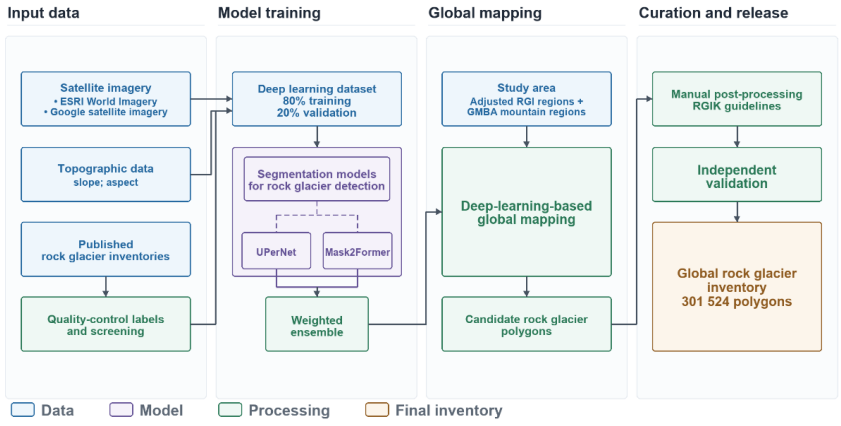


Figure 1. Workflow used to generate the global rock glacier inventory, from study-area delineation and data preparation to model-based candidate generation, manual post-processing, validation, and attribute extraction.

3.1 Study area

The study area for global rock glacier mapping was delineated by combining adjusted Randolph Glacier Inventory (RGI) v7.0 regions (Pfeffer et al., 2014) with the Global Mountain Biodiversity Assessment (GMBA) Mountain Inventory v2 (Körner et al., 2017). The RGI framework provides a globally consistent regional reference for high-latitude and high-mountain cold-climate settings where rock glaciers are known or expected to occur. Because the RGI was developed for glacier studies, it was used pragmatically by retaining mountainous and periglacially relevant parts of the RGI regions, excluding continental ice sheets, extensive low-relief terrain, and other environments unsuitable for rock glacier development, and adding a Western Mediterranean region covering the Sierra Nevada in southern Spain and the Atlas Mountains in North Africa. Within these adjusted regions, the GMBA inventory was used to restrict rock glacier identification, mapping, and spatial analysis to mountainous terrain delineated from elevation, ruggedness, and terrain heterogeneity. This combined RGI-GMBA extent balances global consistency with geomorphological relevance and provides the spatial basis for the inventory. Fig. 2 shows the resulting global study area

https://doi.org/10.5194/essd-2026-575
Preprint. Discussion started: 2 November 2026
© Author(s) 2026. CC BY 4.0 License.



and its two defining spatial layers.

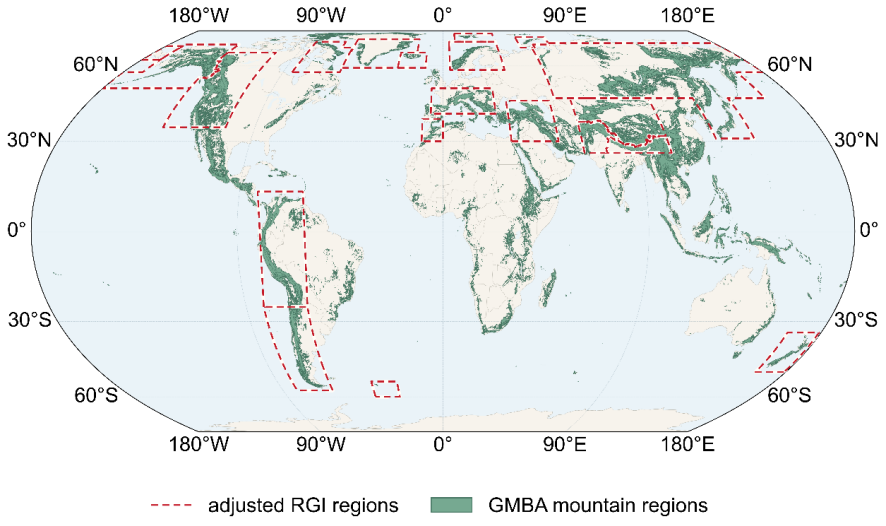


Figure 2. Global study area for rock glacier mapping. Red dashed outlines show the adjusted RGI regions; green polygons show the GMBA mountain regions. Rock glacier identification, mapping, and spatial analysis were restricted to GMBA mountain terrain within the adjusted RGI regions, including the Western Mediterranean extension.

3.2 Rock glacier identification

Two complementary semantic segmentation models were employed for rock glacier identification: a convolutional neural network (CNN)–based architecture, UPerNet, and a Transformer-based architecture, Mask2Former. UPerNet is designed to capture multi-scale spatial features through pyramid pooling, while Mask2Former incorporates global contextual information using self-attention mechanisms. Both models were trained independently using identical training datasets derived from the high-resolution satellite imagery. To integrate the strengths of the two models, their output logits were combined using a weighted ensemble strategy, with equal weights (0.5 and 0.5) assigned to UPerNet and Mask2Former. The ensemble output was subsequently thresholded to generate binary predictions of rock glacier presence.

https://doi.org/10.5194/essd-2026-575
Preprint. Discussion started: 2 November 2026
© Author(s) 2026. CC BY 4.0 License.



The training dataset was constructed by tiling selected representative subregions containing rock glaciers into image patches of 512 × 512 pixels. This procedure resulted in approximately 55 000 image patches, of which about 13 000 contained rock glaciers. To reduce potential classification bias and improve discrimination between rock glaciers and visually similar landforms, an equal number of non-rock-glacier patches were randomly sampled to balance the training dataset. The balanced dataset was randomly split into training (80 %) and validation (20 %) subsets. The intersection over union (IoU) metric was used to evaluate segmentation performance, providing a measure of spatial agreement between predicted and reference rock glacier extents. IoU was computed at the dataset level by aggregating pixel-wise true positives, false positives, and false negatives across the entire dataset.

After training, the ensemble model was applied to the full set of input images to produce spatially continuous predictions. Spatially connected areas predicted as rock glaciers could form a single polygon during vectorization, so one polygon could encompass multiple adjacent rock glacier units. The resulting polygons represent candidate rock glacier locations and extents, which were subsequently subjected to manual inspection and refinement in the following step.

3.3 Manual post-processing

Manual post-processing focused on candidate polygons and generally retained their model-predicted extents.

One experienced rock glacier interpreter conducted manual post-processing using consistent morphological criteria. Visual interpretation was primarily based on high-resolution satellite imagery from ESRI World Imagery, with Google Satellite imagery used where additional detail was needed to resolve ambiguous surface characteristics. The same RGIK morphological criteria used for the training samples guided this review (RGIK, 2023; Brardinoni et al., 2026).

Candidate polygons were evaluated by combining surface texture, overall form and

https://doi.org/10.5194/essd-2026-575
Preprint. Discussion started: 2 November 2026
© Author(s) 2026. CC BY 4.0 License.

Open Access Earth System Science Data Discussions

visible frontal and lateral features. Where boundaries were refined, the extended-footprint convention used for the training samples was retained, with frontal and lateral margins included according to visible landform boundaries. Polygons smaller than 0.01 km^2 were excluded (Sun et al., 2024).

Removal focused on candidate patches lacking coherent geomorphological structure and on features interpreted as debris-covered glaciers or rock avalanches. Near glacier margins, candidates were excluded as debris-covered glaciers only when their visible morphology supported that interpretation, accounting for positional uncertainties in existing glacier inventories.

Boundaries were adjusted where a model-predicted outline differed from a landform boundary discernible in the imagery. Additional features meeting these morphological criteria were added when encountered during inspection of nearby candidate polygons. Model output was retained where visual evidence remained ambiguous. Connected polygons were generally retained as mapped, so the final inventory includes polygons encompassing multiple adjacent rock glacier units.

3.4 Uncertainty assessment

Following manual post-processing, an independent visual assessment evaluated whether mapped polygons met the adopted morphological identification criteria for rock glaciers.

A systematic random subset of 3015 rock glacier polygons (approximately 1% of the inventory) was selected for validation. Each sampled polygon was independently evaluated by two reviewers who were not involved in the mapping or post-processing procedures. All assessments were based on visual interpretation of the same high-resolution satellite imagery sources used throughout the inventory compilation.

For each sampled polygon, reviewers assessed whether its visible features met the adopted morphological identification criteria for rock glaciers. In cases of disagreement,

https://doi.org/10.5194/essd-2026-575
Preprint. Discussion started: 2 November 2026
© Author(s) 2026. CC BY 4.0 License.


the two reviewers jointly re-examined the feature and reached a final consensus classification. Polygons meeting the criteria were treated as true positives and the remaining polygons as false positives for calculating precision relative to this morphological assessment.

Precision (positive predictive value) was calculated as the proportion of sampled polygons judged to meet these criteria. Estimating recall, the F1 score, and inventory completeness requires an independent assessment of unmapped areas.

Spatial correspondence was assessed by comparing the global inventory with selected regional rock glacier inventories from the eastern European Alps (Kellerer-Pirklbauer et al., 2012), Greater Caucasus (Tielidze et al., 2023), Tibetan Plateau (Sun et al., 2024), northeastern Yakutia (Lytkin, 2020), contiguous United States (Johnson et al., 2021), Argentine Andes (IANIGLA, 2018), and Peruvian Andes (Medina et al., 2026), and with the RoGI dataset from 12 selected study areas across five continents (Rouyet et al., 2025) (Tables 2 and 3).

Comparisons for the eastern European Alps, Greater Caucasus, Tibetan Plateau, northeastern Yakutia, contiguous United States, and Argentine Andes used the regional subsets assembled for this study. The PRoGI v1.0 comparison included all 2338 extended-footprint polygons. The RoGI v2.0 comparison included 335 extended-footprint polygons associated with landforms classified as certain in the reference dataset within the 12 supplied study-area boundaries; one polygon associated with an uncertain landform was excluded.

For each comparison, the reference and global inventory polygons were evaluated within the same comparison region. Areas were calculated in an equal-area projection after merging overlapping polygons within each inventory to avoid double counting. The intersection of the two polygon unions was calculated and expressed relative to the area of each inventory. Reference polygons retained their original size range. For RoGI, comparisons were conducted for each of the 12 study areas and overall.

https://doi.org/10.5194/essd-2026-575
Preprint. Discussion started: 2 November 2026
© Author(s) 2026. CC BY 4.0 License.



3.5 Final dataset assembly and environmental statistics

After manual post-processing and validation, the retained polygons were compiled into the final release layer. Geometry checks were performed to remove empty geometries, repair invalid polygons where possible, and identify duplicate or overlapping features introduced during tiling and mosaicking. Polygon areas were calculated using an equal-area projection, whereas the released polygon geometries and centroid coordinates (longitude and latitude) are provided in WGS 84 geographic coordinates (EPSG:4326). All reported regional totals were derived from the cleaned release layer.

Regional and global environmental summaries were calculated by overlaying the inventory outlines with the topographic and climatic rasters. Raster values within the mapped footprints were grouped by variable class, and the area represented by the raster cells was summed within each class. Aspect was grouped into eight directional classes (N, NE, E, SE, S, SW, W, and NW). The association with the PZI permafrost-potential domain was evaluated on this raster-area basis.

The release is versioned to distinguish it from future updates. Any subsequent corrections or extensions, such as improved regional completeness, activity-state attribution, or revised boundaries based on new imagery, should be released as new versioned products with the archived dataset retained as a stable reference.

4 Results

4.1 Global rock glacier inventory

The global inventory comprises 301 524 mapped polygon features interpreted as rock glacier units or systems, covering a total area of 38 849 km^2. The mapped area is unevenly distributed across the 19 regions. High Mountain Asia (Central Asia and South Asia West and East) accounts for 67.3 % of the total mapped area, followed by the North American Cordillera (Alaska and Western Canada and USA) with 13.6 %, North Asia with 9.5 %, and the Andes (Northern and Southern Andes) with 4.5 %. The

https://doi.org/10.5194/essd-2026-575
Preprint. Discussion started: 2 November 2026
© Author(s) 2026. CC BY 4.0 License.



425 remaining regions collectively contribute 5.1 % (Fig. 3).

The principal output of this study is the released polygon layer itself. Each polygon represents a mapped rock glacier landform or connected rock glacier system interpreted under a consistent global delineation philosophy. The dataset is intended to support both feature-level analyses, such as extracting local topographic or climatic conditions, and
430 regional synthesis, such as comparing mapped area, density, and environmental distributions among mountain systems.

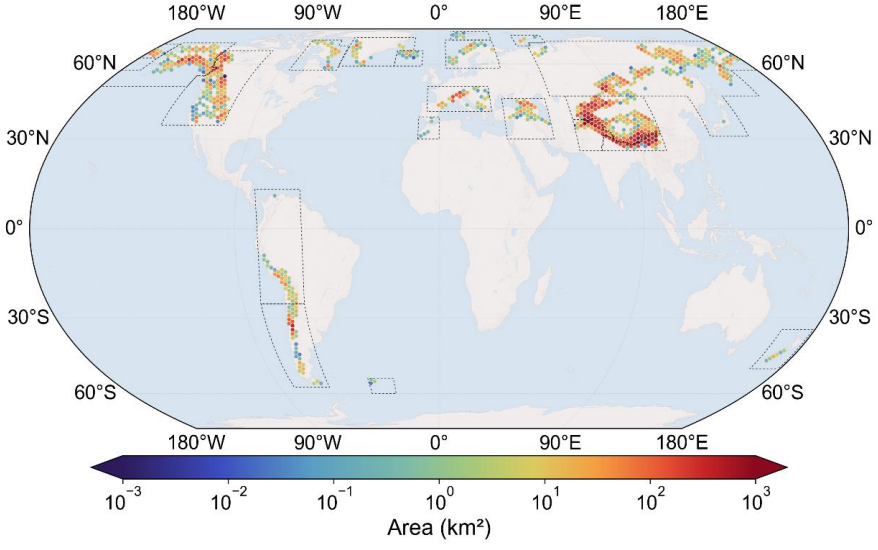


Figure 3. Spatial distribution of mapped rock glaciers in the inventory by reporting region.

435 4.2 Spatial patterns of topographic and climatic attributes

The spatial patterns of topographic and climatic attributes show that mapped rock glaciers occupy a broad but structured environmental envelope (Fig. 4). Elevation exhibits the clearest geographic gradient. In high-latitude mountain regions, rock glaciers occur at relatively low elevations, in many cases below 1000 m a.s.l. and locally
440 close to sea level. Toward the mid-latitudes, mapped elevations commonly shift into approximately 1500–3500 m, whereas in the Andes, High Mountain Asia, and other

https://doi.org/10.5194/essd-2026-575
Preprint. Discussion started: 2 November 2026
© Author(s) 2026. CC BY 4.0 License.


low- to mid-latitude mountain belts they are concentrated mostly above 4000 m and locally extend beyond 5500 m.

Slope and aspect show more consistent global organization than elevation. Most mapped polygons occur on moderately inclined terrain, commonly around 10–25°, while very gentle terrain (<5°) and very steep slopes (>30°) are comparatively uncommon. Aspect shows a clear hemispheric structure: poleward-facing sectors are prominent in both hemispheres, with north-facing components dominating many Northern Hemisphere regions and south-facing components more evident in the Southern Hemisphere.

The climatic layers distinguish major mountain systems in more detail. MAAT values are lowest in circum-Arctic mountain regions, frequently below −15 °C, whereas rock glaciers in High Mountain Asia are generally associated with less extreme but still negative MAAT values, commonly around −10 to −5 °C. MAGT is shifted toward warmer values than MAAT, remaining mostly negative in Arctic settings but clustering near the freezing point in many mid-latitude mountain systems and locally becoming positive along parts of the Andes and the margins of High Mountain Asia. Annual precipitation also shows strong regional contrasts: interior mountain belts of Central Asia and western North America include relatively dry settings below about 600–800 mm, while maritime, island, and monsoon-influenced mountain systems often exceed 1000–1500 mm and locally surpass 2000 mm.

https://doi.org/10.5194/essd-2026-575
Preprint. Discussion started: 2 November 2026
© Author(s) 2026. CC BY 4.0 License.

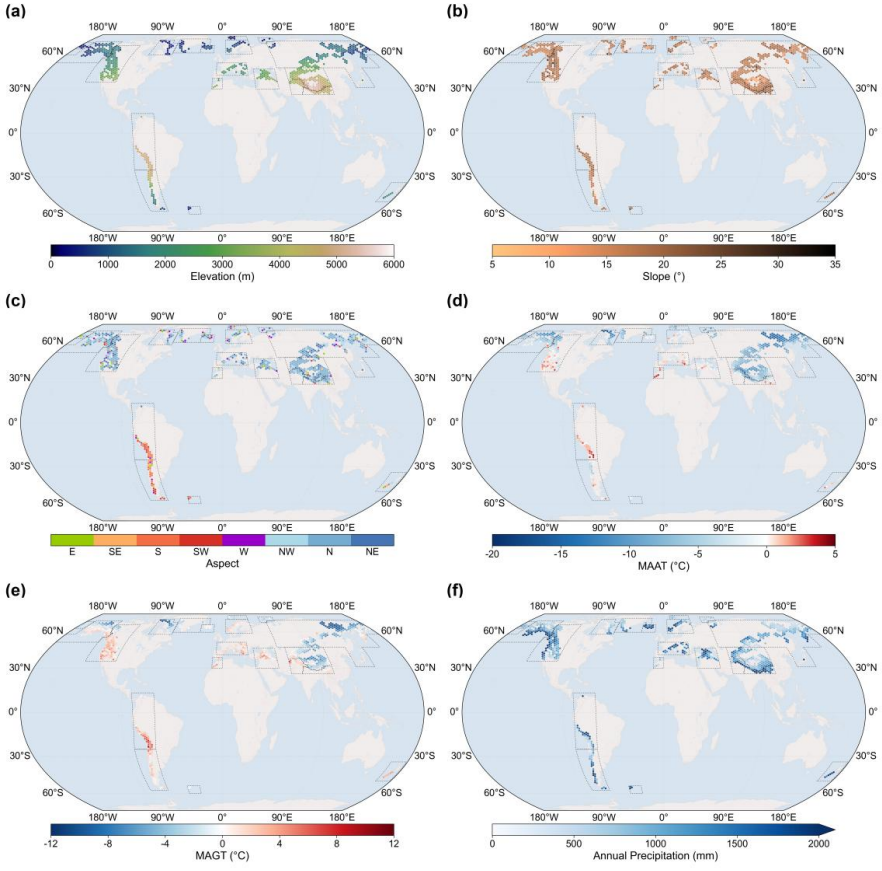


Figure 4. Spatial patterns of topographic and climatic attributes associated with mapped rock glaciers. (a) Mean elevation (m a.s.l.); (b) mean slope (°); (c) modal aspect class; (d) mean annual air temperature (MAAT, °C); (e) mean annual ground temperature (MAGT, °C); and (f) mean annual precipitation (mm).

4.3 Area-weighted global distributions of environmental variables

Area-weighted distributions describe the environmental conditions represented by mapped rock glacier area (Fig. 5).

https://doi.org/10.5194/essd-2026-575
Preprint. Discussion started: 2 November 2026
© Author(s) 2026. CC BY 4.0 License.

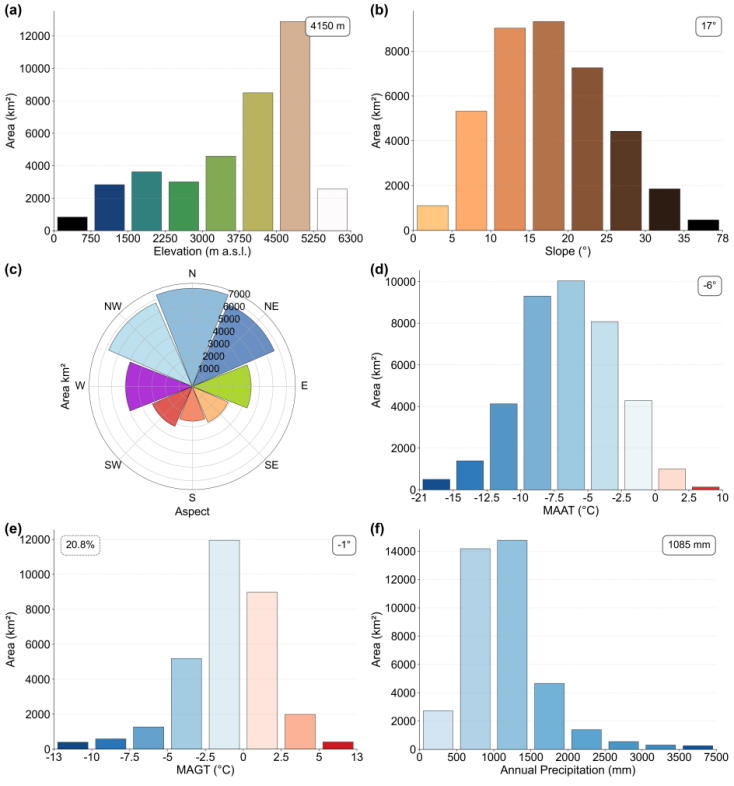


Figure 5. Area-weighted global distributions of environmental variables associated with mapped rock glaciers. (a) Elevation (m a.s.l.); (b) slope (°); (c) aspect; (d) mean annual air temperature (MAAT, °C); (e) mean annual ground temperature (MAGT, °C); and (f) mean annual precipitation (mm). Bars indicate mapped rock glacier area within each class interval. Panel annotations show the proportion of missing data (upper left) and the area-weighted median (upper right), where applicable.

The area-weighted topographic distributions indicate that most mapped rock glacier area is concentrated in high-elevation mountain terrain and on moderate slopes. The median elevation is approximately 4150 m a.s.l., with the largest area contribution between 3750 and 5250 m. The median slope is approximately 17°, and most mapped area falls between 5° and 25°. Poleward-facing sectors make up the largest share of mapped area, consistent with an influence of topographic shading and radiation

https://doi.org/10.5194/essd-2026-575
Preprint. Discussion started: 2 November 2026
© Author(s) 2026. CC BY 4.0 License.


contrasts.

Thermal variables show that mapped rock glacier area is mainly associated with cold to near-freezing conditions. The area-weighted median MAAT is approximately −6 °C, with the largest area contribution between −10 and −5 °C. Modeled MAGT is shifted toward warmer values, with a median of approximately −1 °C and a dominant interval near the freezing point.

Precipitation spans a wide range but is concentrated in intermediate classes. The area-weighted median annual precipitation is approximately 1085 mm, and the largest area contribution occurs between 800 and 1500 mm. Very dry and very wet settings are both represented, but they account for smaller fractions of the mapped area. Together, the area-weighted distributions indicate that the global inventory is dominated by high-elevation, moderately sloping, poleward-oriented landforms under cold to near-freezing and moderately moist environmental conditions.

4.4 Uncertainty and validation

A total of 3015 mapped polygons, corresponding to approximately 1 % of the global inventory, were independently examined as part of the uncertainty assessment. Of these, 2741 polygons met the adopted morphological identification criteria for rock glaciers, and the remaining 274 were classified as inconsistent with these criteria. The resulting precision was 90.9 %.

The 95 % confidence interval for this proportion, calculated using the Wilson score method, was 89.8 %–91.9 % (Wilson, 1927).

4.5 Modeling performance

Fig. 6 summarizes the model behaviour used for candidate generation. The training and validation IoU curves for UPerNet and Mask2Former show stable convergence and broadly consistent validation performance, indicating that the models provide a useful automated screening step for identifying candidate rock glacier extents.

https://doi.org/10.5194/essd-2026-575
Preprint. Discussion started: 2 November 2026
© Author(s) 2026. CC BY 4.0 License.



These diagnostics describe model performance relative to the training and validation labels. The independent visual assessment evaluates the inventory after manual post-processing against the adopted morphological criteria.

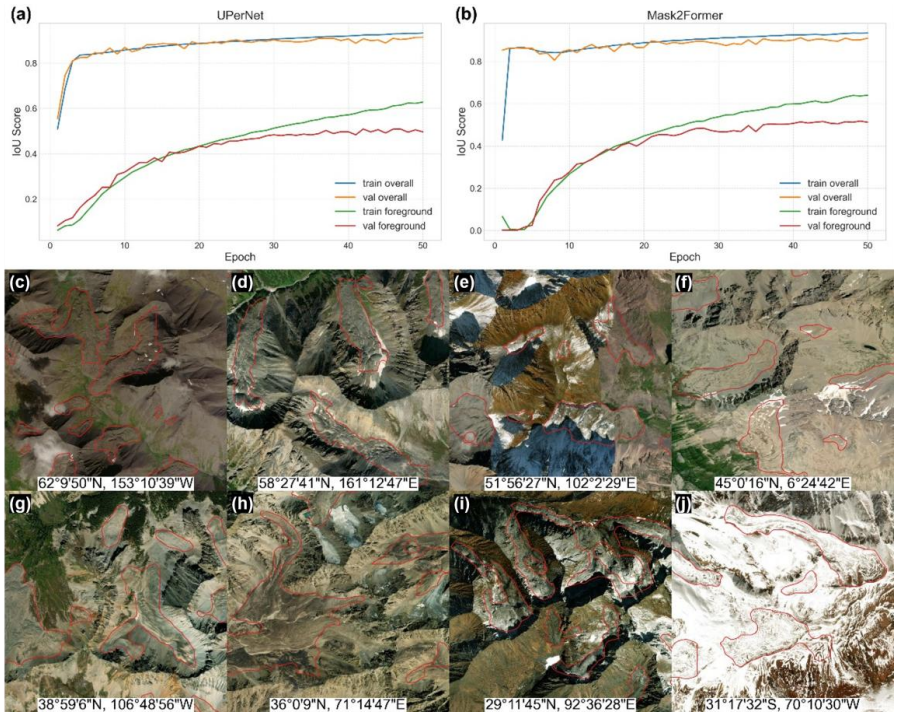


Figure 6. Performance of the deep-learning-based candidate-generation models. (a-b) Training and validation IoU curves for UPerNet and Mask2Former. (c-j) Representative prediction examples; red outlines indicate model-derived candidate boundaries. Basemap: World Imagery (Powered by Esri).

https://doi.org/10.5194/essd-2026-575
Preprint. Discussion started: 2 November 2026
© Author(s) 2026. CC BY 4.0 License.



4.6 Comparison with existing regional inventories

Table 2. Spatial correspondence between selected regional rock glacier inventories and the global inventory. N_ref denotes the number of reference polygon features before merging; each feature may represent one landform or a connected system. Area_ref and Area_inv are the reference and global inventory union areas within each comparison region, and Area_ov is their intersection area. Ov./Ref. = 100 × Area_ov / Area_ref; Ov./Inv. = 100 × Area_ov / Area_inv.

Region	N_ref	Area_ref (km^2)	Area_inv (km^2)	Area_ov (km^2)	Ov./Ref. (%)	Ov./Inv. (%)
eastern European Alps	1 647	118.93	75.19	38.11	32.0	50.7
Greater Caucasus	1 461	297.72	418.00	179.37	60.2	42.9
Tibetan Plateau	44 273	6067.33	14186.07	4353.75	71.8	30.7
northeastern Yakutia	4 503	223.71	774.71	90.21	40.3	11.6
contiguous United States	10 332	1004.05	901.49	541.61	53.9	60.1
Argentine Andes	8 454	951.96	1097.26	561.35	59.0	51.2
Peruvian Andes	2 338	93.81	193.86	58.44	62.3	30.1

Across the seven comparisons in Table 2, Ov./Ref. ranged from 32.0 % in the eastern European Alps to 71.8 % on the Tibetan Plateau, and Ov./Inv. ranged from 11.6 % in northeastern Yakutia to 60.1 % in the contiguous United States. For PRoGI, the overlapping area was 58.44 km^2, with Ov./Ref. of 62.3 % and Ov./Inv. of 30.1 %. For RoGI (Table 3), the total overlapping area was 22.51 km^2, with Ov./Ref. of 77.0 % and Ov./Inv. of 50.0 %. Within RoGI, Ov./Ref. varied among the 12 study areas, from 0 % in Nordenskiöld Land to 92.2 % in the Central Andes.

https://doi.org/10.5194/essd-2026-575
Preprint. Discussion started: 2 November 2026
© Author(s) 2026. CC BY 4.0 License.



Table 3. Spatial correspondence between RoGI and the global inventory for the 12 study areas and overall. Metrics are defined in Table 2. A dash denotes an undefined Ov./Inv. when Area_inv = 0.

Study area	N_ref	Area_ref (km²)	Area_inv (km²)	Area_ov (km²)	Ov./Ref. (%)	Ov./Inv. (%)
Carpathians	18	1.19	0.92	0.73	61.3	78.8
Western Alps	30	0.94	1.05	0.59	62.5	55.9
Troms	14	1.03	2.12	0.85	82.3	40.0
Finnmark	17	0.83	1.35	0.66	78.7	48.6
Nordenskiöld Land	18	0.72	0.00	0.00	0.0	–
Vanoise Massif	49	1.70	2.71	1.20	70.4	44.3
Southern Venosta	39	1.79	1.46	1.11	62.1	75.9
Disko Island	29	6.51	12.49	4.68	71.9	37.5
northern Tien Shan	14	4.88	6.78	4.31	88.2	63.5
Brooks Range	14	0.95	1.53	0.53	55.5	34.5
central Andes	69	8.07	13.89	7.44	92.2	53.5
Southern Alps	24	0.63	0.74	0.42	67.2	57.4
Overall	**335**	**29.24**	**45.05**	**22.51**	**77.0**	**50.0**

5 Discussion

5.1 Global distribution patterns of rock glaciers

5.1.1 Climatic and topographic gradients

Mapped rock glacier area is concentrated in High Mountain Asia, the North American Cordillera, northern Eurasia, and the Andes. This spatial structure is consistent with the coincidence of cold mountain terrain, high relief, debris supply, and permafrost-favorable conditions across large areas. Regional and near-global syntheses have identified the same broad mountain and high-latitude settings as principal rock glacier environments (Barsch, 1996; D. B. Jones et al., 2018). The global inventory quantifies the relative contributions of these regions to mapped rock glacier area and characterizes the associated topographic and climatic conditions.

https://doi.org/10.5194/essd-2026-575
Preprint. Discussion started: 2 November 2026
© Author(s) 2026. CC BY 4.0 License.



The elevation-latitude gradient provides the clearest climatic interpretation of the mapped distribution. Low-elevation Arctic and sub-Arctic occurrences and high-elevation occurrences in the Andes and High Mountain Asia represent regional expressions of similar thermal constraints on ice-rich debris. Regional lower limits reflect latitude, continentality, radiation balance, and topographic modification of ground temperature (Ran and Liu, 2018; Millar and Westfall, 2019).

The concentration of mapped area on moderate gradients is consistent with debris accumulation and creep requiring sufficient driving stress while maintaining landform coherence. Very gentle slopes limit deformation, and very steep slopes favor rapid mass wasting and short residence times (Onaca et al., 2017; Abdullah and Romshoo, 2024; Sun et al., 2024).

The hemispheric reversal in predominant mapped slope orientation is consistent with reduced incoming solar radiation, longer snow persistence, and cooler ground conditions on poleward-facing slopes. This pattern supports the interpretation that local radiation balance modulates rock glacier distribution within the broader climatic envelope (Kellerer-Pirklbauer et al., 2012; Johnson et al., 2021; Remya et al., 2024).

Thermal and hydroclimatic attributes define the climatic envelope of mapped rock glacier area. Negative MAAT and near-freezing MAGT are consistent with cold-ground conditions, and regional precipitation differences may influence snow supply, ice formation, vegetation cover, and surface preservation. The concentration under intermediate precipitation is compatible with a role for moisture supply in ice preservation and debris-ice coupling. Very wet settings are more likely to support glacierization, dense vegetation, or rapid reworking that obscures morphology (Rangecroft et al., 2015; Charbonneau and Smith, 2018; Schaffer et al., 2019). High Mountain Asia accounts for 67.3 % of the mapped area and therefore has the greatest influence on these global area-weighted distributions. Interpreting regional differences also requires information on lithology, debris supply, glacier history, snow

https://doi.org/10.5194/essd-2026-575
Preprint. Discussion started: 2 November 2026
© Author(s) 2026. CC BY 4.0 License.



redistribution, and activity state.

5.1.2 Relationship with global permafrost

The PZI represents broad climatic conditions favorable for permafrost (Gruber, 2012). Approximately 91.8 % of the mapped area falls within the PZI permafrost-potential domain (Fig. 7). This broad agreement with modeled permafrost zonation is consistent with the use of rock glaciers as geomorphological indicators of mountain permafrost.

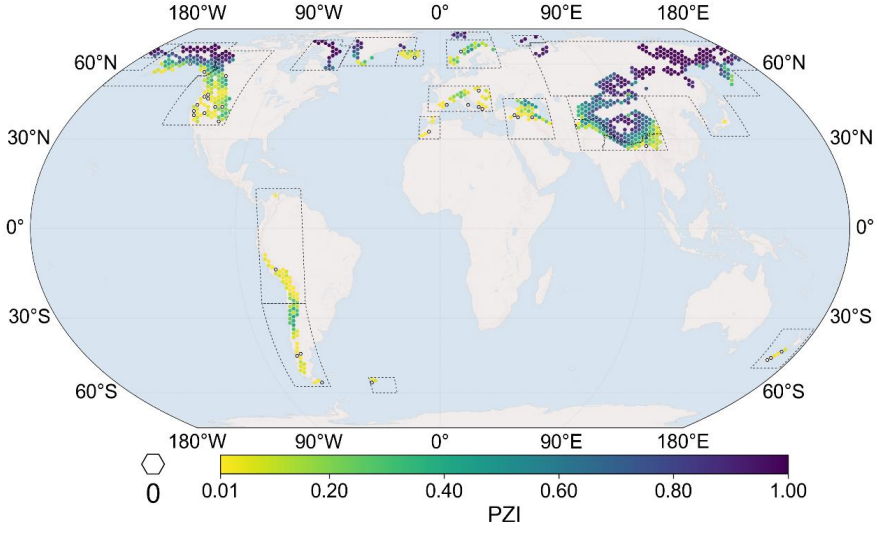


Figure 7. Regional distribution of the Global Permafrost Zonation Index (PZI) associated with mapped rock glaciers. Higher PZI values indicate more widespread potential permafrost occurrence, while lower values indicate occurrence restricted to locally favorable conditions.

The remaining 8.2 % of mapped area lies outside the PZI permafrost-potential domain. Topographic shading, cold-air pooling, snow redistribution, and debris-cover insulation can produce local ground conditions that are poorly resolved by global statistical permafrost models (Janke et al., 2012). Landforms shaped by past permafrost creep can also retain recognizable morphology after ground ice has degraded (Kofler et al., 2020). Local thermal and kinematic observations, together with a review of the mapped

https://doi.org/10.5194/essd-2026-575
Preprint. Discussion started: 2 November 2026
© Author(s) 2026. CC BY 4.0 License.


outlines, would help assess whether these differences reflect local permafrost conditions, preserved morphology, or mapping errors.

High-latitude mountain systems and continental high-elevation regions, including northern Eurasia, Alaska, and High Mountain Asia, generally align with medium-to-high PZI classes. Semi-arid and mid- to low-latitude mountain belts show broader spreads toward lower PZI values, consistent with possible local influences of elevation, aspect, and topographic microclimate in climatically marginal settings. The inventory complements model-based permafrost products by identifying landforms that can guide targeted validation.

5.2 Interpretation of inventory-comparison differences

Comparisons with the seven regional inventories distinguish agreement in total mapped area from spatial correspondence. In each of the contiguous United States and Argentine Andes comparisons, the global inventory and the corresponding reference inventory have similar total mapped areas, while overlap accounts for approximately 51 %–60 % of the area of each inventory. Total area alone therefore gives an incomplete description of agreement between their mapped footprints. The global inventory has a smaller area than the eastern European Alps reference inventory and a larger area than the northeastern Yakutia reference inventory. On the Tibetan Plateau and in the Peruvian Andes, overlap covers more than 60 % of reference area but approximately 30 % of global-inventory area, indicating substantial inclusion of previously mapped areas alongside extensive areas outside the reference outlines. In the Greater Caucasus, the corresponding fractions are 60.2 % and 42.9 %, with substantial areas unique to each inventory. Comparisons with inventories that also supplied training samples additionally measure consistency with the source mapping.

RoGI provides a complementary comparison across 12 local study areas mapped within a common inventorying framework. The aggregate Ov./Ref. of 77.0 % for RoGI is weighted by reference area, while individual study-area values range from

https://doi.org/10.5194/essd-2026-575
Preprint. Discussion started: 2 November 2026
© Author(s) 2026. CC BY 4.0 License.



0 % to 92.2 %. The global inventory contains 109 polygon features in Svalbard, with a union area of 9.79 km². Inspection of model predictions showed that the model did not detect the features recorded in the Nordenskiöld Land reference inventory, where 18 polygons cover approximately 0.72 km². This non-overlapping reference area represents 6.9 % of the combined area of the mapped Svalbard polygons and these reference polygons. Two reference polygons fall below the global inventory minimum of 0.01 km²; the remaining 16 cover approximately 0.71 km² and meet its size criterion. These above-threshold reference polygons indicate a local gap in model detection that remained after manual post-processing. Manual additions depended on encountering features during candidate review.

Finer imagery and terrain data can reveal additional landforms and internal units while substantial differences in mapped area persist among interpreters (Brardinoni et al., 2019). The common 2.4 m working resolution in this study standardizes the input grid; native image detail, regional image quality, acquisition season, and mosaic composition determine the information available for interpretation. Published inventory studies document obscuration by snow, shadow, and vegetation, together with positional differences between image sources (Tielidze et al., 2023; Sun et al., 2024; Rouyet et al., 2025). These conditions may contribute to regional differences in recognition and delineation. The published eastern European Alps inventory classifies approximately 79 % of its units as relict and identifies forest cover as an obstacle to their detection (Kellerer-Pirklbauer et al., 2012). Repeated delineation of relict examples also showed substantial differences at subdued fronts, upslope transitions, and adjacent lobes (Brardinoni et al., 2019). These difficulties may partly explain the lower overlap in this region (Ov./Ref. = 32.0 %). The United States reference, by comparison, includes only landforms interpreted as active from morphology (Johnson et al., 2021), so the regional comparisons involve different mixtures of morphological types. Boundary conventions further affect the surfaces included: the Yakutia reference calculates area excluding slopes (Lytkin, 2020), whereas our RGIK-based extended footprints include frontal and

https://doi.org/10.5194/essd-2026-575
Preprint. Discussion started: 2 November 2026
© Author(s) 2026. CC BY 4.0 License.



lateral slopes (RGIK, 2023; Brardinoni et al., 2026). This difference may contribute to the larger global-inventory area in Yakutia. Even with extended outlines, repeated delineation of 400 PRoGI landforms showed greater disagreement for large composite systems and the inclusion of secondary lobes (Medina et al., 2026). Such differences in the extent assigned to a landform may also contribute to partial overlap between inventories that share broad identification and delineation principles.

The interpretation embodied in training samples can also influence automated mapping. Some source inventories identify active landforms using detectable movement, while others combine morphology and kinematics to represent a wider range of activity states (Wang et al., 2017; Rouyet et al., 2021). Reinterpreting selected samples under common criteria harmonizes their outlines; the morphologies available for learning still depend on sample composition. Our samples span ten regions, with the largest contribution from the Tibetan Plateau, and were selected from imagery suitable for interpretation. Training on active-landform morphology can limit recognition of subdued, vegetated relict forms (Hu et al., 2023). Missed detections outside training areas have also been linked to poorly developed morphological features (Sun et al., 2024). Sparsely represented morphologies and image conditions may similarly contribute to differences in regional detection here. Ambiguous rooting-zone labels have also been associated with less certain predicted boundaries than well-defined fronts (Erharter et al., 2022). The validation curves in Fig. 6 characterize performance on held-out patches from the sampled subregions; the regional inventory comparisons additionally assess correspondence across the comparison regions. Mapping scale affects the size of landforms retained, boundary detail, and the subdivision of connected systems (RGIK, 2023; Brardinoni et al., 2026). During RoGI compilation, differences in initial digitizing scale affected outline detail and the sizes of landforms considered (Rouyet et al., 2025). Our 0.01 km² minimum is consistent with the RGIK recommendation for global inventories and is also used in the Greater Caucasus and Tibetan Plateau references, whereas PRoGI retains smaller landforms (Tielidze et al., 2023; Sun et al.,

https://doi.org/10.5194/essd-2026-575
Preprint. Discussion started: 2 November 2026
© Author(s) 2026. CC BY 4.0 License.

Open Access Earth System Science Data Discussions

2024; Medina et al., 2026). All reference inventories retain their original size ranges in our comparisons. Reference area below the cutoff can reduce Ov./Ref. where it falls outside the global mapped footprint. Semantic segmentation can join adjacent units into one polygon (Sun et al., 2024). Splitting or merging a fixed outer footprint changes feature counts and individual areas while preserving union area and overlap; including different lobes, connecting areas, or outer slopes changes the area comparison.

The 90.9 % feature-level precision assessed against the adopted morphological criteria and the variable area overlap with regional inventories characterize different aspects of the mapped product. A polygon can meet the identification criteria while its outline differs from a reference delineation; differences in the landforms included also affect overlap. Interpretation by one experienced operator provides a common basis for mapping, with ambiguous cases remaining sensitive to individual judgement. RGIK recommends additional-operator review to reconcile such differences (Brardinoni et al., 2026). Our two reviewers assessed morphological identification, while repeated delineation would additionally quantify boundary variability. The overlap fractions depend on the total area of each inventory: a larger global mapped extent can yield substantial coverage of the reference inventory together with a smaller fraction of global-inventory area overlapping the reference. Boundary differences have been shown to alter derived elevation ranges (Brardinoni et al., 2019), and regional differences in detection and delineation may also affect the contributions of mountain systems and environmental settings to our global area-weighted distributions. Our unified framework is intended to limit differences introduced by data preparation, interpretation criteria, mapping methods, and scale choices, providing a common basis for comparing rock glacier distributions and their environmental relationships across regions.

https://doi.org/10.5194/essd-2026-575
Preprint. Discussion started: 2 November 2026
© Author(s) 2026. CC BY 4.0 License.



5.3 Potential water-storage magnitude

The water-storage calculation is a sensitivity analysis linked to mapped area. The two-dimensional inventory constrains landform extent; water-equivalent interpretation requires assumptions about thickness, internal ice content, and activity state. Empirical thickness-area scaling relationships, such as those proposed by Brenning (2005) and applied at global scale by Jones et al. (2018), provide a transparent first-order scenario.

Applying the Brenning (2005) thickness-area relation, following the global-scale implementation of Jones et al. (2018), gives an order-of-magnitude storage scenario for the expanded mapped area. Under an assumed ice content fraction of 40–60 % (mean 50 %) and standard density conversion from ice to water equivalent, this scenario yields approximately 539–808 Gt, with a central illustrative value of about 674 Gt. The value indicates the magnitude implied by one explicit parameter set and remains separate from the released inventory product.

For context, estimated global glacier water equivalent outside the Greenland and Antarctic ice sheets is approximately 145 000 ± 38 000 Gt (Farinotti et al., 2019). The illustrative rock glacier storage estimate is small relative to global glacier water storage. Its scientific relevance lies in regional hydrology: in arid and semi-arid mountains, rock glaciers can represent persistent ice-rich landforms during glacier retreat (Rangecroft et al., 2015; Schaffer et al., 2019).

The expanded mapped extent contributes to the higher value relative to Jones et al. (2018). Under the non-linear thickness-area relation, the estimate also depends on how the mapped area is divided among polygons.

The main sources of uncertainty include polygon-landform correspondence, non-linear scaling, unknown activity state, variable ice content, and limited thickness observations. Units with ice contents below the assumed range, including ice-depleted relict landforms, would reduce storage relative to the scenario. The adopted thickness-area relation assigns greater thickness to larger landforms. Applying it to a polygon

https://doi.org/10.5194/essd-2026-575
Preprint. Discussion started: 2 November 2026
© Author(s) 2026. CC BY 4.0 License.


encompassing several adjacent rock glaciers therefore yields a larger volume than summing separate estimates for those landforms, even when total area and assumed ice content are unchanged.

Robust volume estimates require activity-state classification, regionally calibrated thickness models, explicit ice-content assumptions, and targeted geophysical or field observations. The 539–808 Gt range expresses the sensitivity of global storage to the stated ice-content assumptions; regional water-resource assessment requires locally constrained estimates.

5.4 Dataset perspectives and future directions

The inventory is best used as a harmonized occurrence and landform-extent baseline. Appropriate applications include global and cross-regional comparison, exploratory analysis of topographic and climatic settings, prioritization of areas for local inventory improvement, and first-order overlay with mountain permafrost or hydrological datasets. Comparisons based on polygon counts or individual-polygon attributes should account for the representation of connected landforms.

Activity state, individual-landform volume, and site-scale hazard assessment require additional observations, including ground temperature, movement, subsurface ice content, local geomorphic context, and survey-specific mapping criteria. High-resolution regional inventories, field validation, and kinematic observations remain essential for those applications.

Future releases should refine mapped boundaries and document regional differences in interpretation and boundary placement alongside changes to the inventory. Delineating individual rock glaciers within connected systems and determining their planform morphology and upslope connection type require interpretation of their relationships with the surrounding terrain and debris-source areas. The diversity of landform shapes and connections across mountain environments poses a challenge to consistent characterization of these attributes across regions. Future work could explore

https://doi.org/10.5194/essd-2026-575
Preprint. Discussion started: 2 November 2026
© Author(s) 2026. CC BY 4.0 License.



multimodal foundation models for joint interpretation of imagery, terrain, and geomorphological context to improve individual delineation and attribute identification, supporting comparative studies of rock glacier morphology and its environmental setting. These connection classes describe visible spatial relationships; interpretations of genesis require additional geomorphological evidence (Brardinoni et al., 2026). Reliable kinematic observations would improve activity attribution and allow regional comparisons to distinguish currently moving landforms from those with little detectable movement. Activity-state information would support validation and refinement of mountain permafrost distribution models. Recording imagery, training data, assessment design, attribute definitions, and version-specific regional changes would preserve comparability as the inventory is refined.

6 Data availability

The Global Rock Glacier Inventory is publicly available through the National Tibetan Plateau / Third Pole Environment Data Center at https://doi.org/10.11888/Cryos.tpdc.303562 (Xu et al., 2026). A product guide is available at https://github.com/radiofor/Global-Rock-Glacier-Inventory and provides instructions for downloading and using the regional files and interpreting their attributes.

7 Conclusion

This study presents a globally harmonized rock glacier inventory comprising 301 524 mapped polygons with a total area of 38 849 km^2 across high-mountain and high-latitude regions worldwide. Built under a single globally consistent mapping framework and assessed through independent visual review against the adopted morphological criteria, the dataset provides a common global reference for evaluating rock glacier occurrence, mapped area, and environmental setting. Mapped rock glaciers are widespread across high-mountain and high-latitude environments, with mapped area concentrated in High Mountain Asia, the North American Cordillera, North Asia, and

https://doi.org/10.5194/essd-2026-575
Preprint. Discussion started: 2 November 2026
© Author(s) 2026. CC BY 4.0 License.



the Andes. Mapped rock glaciers generally occur at higher elevations toward lower latitudes. Their area-weighted environmental distributions are characterized by moderate slopes, poleward-facing aspects, negative air temperatures, near-freezing modeled ground temperatures, and intermediate precipitation regimes. Their broad association with modeled permafrost-potential terrain provides a check of environmental consistency and indicates that the inventory can support evaluation of mountain permafrost indicators as a geomorphic occurrence dataset. Comparisons with regional inventories further document agreement in mapped extent and identify regional differences in the recorded distribution. In areas where mapped rock glaciers occur outside modeled permafrost-potential terrain, regional investigation should consider local ground conditions influenced by topographic shading, cold-air pooling, and debris-cover insulation, as well as landforms preserved from past permafrost creep. For rock glacier water storage, the sensitivity calculation suggests a potential global magnitude of approximately 539–808 Gt (central illustrative value of about 674 Gt), providing a first-order storage scenario that is small relative to global glacier water equivalent. Rock glaciers may serve as locally important long-term ice and water stores; their contribution to regional water resources depends on local ice content and hydrological connectivity. With standardized attributes, validation information, and open access, the inventory enables cross-regional comparison and helps prioritize field and kinematic observations to investigate subsurface ice, long-term water storage, and permafrost-related geomorphic activity in deglaciating mountain systems.

Author contributions. MF and JX conceived and designed the study. JX developed the methodology, performed the analysis, and wrote the original draft. MF provided continuous guidance throughout the study and edited and finalized the manuscript. QW and PZ contributed to data processing. YS, DY, and XZ contributed to manuscript revision. XL reviewed the final manuscript and provided final comments and approval

https://doi.org/10.5194/essd-2026-575
Preprint. Discussion started: 2 November 2026
© Author(s) 2026. CC BY 4.0 License.



before submission. All authors reviewed and approved the final manuscript.

Competing interests. The authors declare that they have no conflict of interest.

Financial support. This work was supported by the National Key Research and Development Program of China: [grant number 2023YFF0725005].

References

Abdullah, T. and Romshoo, S. A.: A Comprehensive Inventory, Characterization, and Analysis of Rock Glaciers in the Jhelum Basin, Kashmir Himalaya, Using High-Resolution Google Earth Data, Water, 16, https://doi.org/10.3390/w16162327, 2024.

Ballantyne, C. K.: Periglacial geomorphology, John Wiley & Sons, 2001.

Barsch, D.: Rockglaciers: indicators for the present and former geoecology in high mountain environments, Springer Science & Business Media, Heidelberg, Germany, 331 pp., 1996.

Blöthe, J. H., Rosenwinkel, S., Höser, T., and Korup, O.: Rock-glacier dams in High Asia, Earth Surf Process Landf, 44, 808–824, https://doi.org/10.1002/esp.4532, 2019.

Boeckli, L., Brenning, A., Gruber, S., and Noetzli, J.: A statistical approach to modelling permafrost distribution in the european alps or similar mountain ranges, Cryosphere, 6, 125–140, https://doi.org/10.5194/tc-6-125-2012, 2012.

Brardinoni, F., Scotti, R., Sailer, R., and Mair, V.: Evaluating sources of uncertainty and variability in rock glacier inventories, Earth Surf Process Landf, 44, 2450–2466, https://doi.org/10.1002/esp.4674, 2019.

Brardinoni, F., Vivero, S., Barboux, C., Bodin, X., Cicoira, A., Echelard, T., Hu, Y., Jones, N., Lambiel, C., MacDonell, S., Pellet, C., Rouyet, L., Ruiz, L., Schaffer, N., Wehbe, M., and Delaloye, R.: RGIK guidelines for compiling consistent rock glacier inventories, Geomorphology, 492, 110050, https://doi.org/10.1016/j.geomorph.2025.110050, 2026.

Brenning, A.: Geomorphological, hydrological and climatic significance of rock glaciers in the Andes of Central Chile (33–35°S), Permafr Periglac Process, 16, 231–240, https://doi.org/10.1002/ppp.528, 2005.

Brighenti, S., Tolotti, M., Bruno, M. C., Engel, M., Wharton, G., Cerasino, L., Mair, V.,

https://doi.org/10.5194/essd-2026-575
Preprint. Discussion started: 2 November 2026
© Author(s) 2026. CC BY 4.0 License.



and Bertoldi, W.: After the peak water: the increasing influence of rock glaciers on alpine river systems, Hydrological Processes, 33, 2804–2823, https://doi.org/10.1002/hyp.13533, 2019.

Brighenti, S., Hotaling, S., Finn, D. S., Fountain, A. G., Hayashi, M., Herbst, D., Saros, J. E., Tronstad, L. M., and Millar, C. I.: Rock glaciers and related cold rocky landforms: Overlooked climate refugia for mountain biodiversity, Glob Chang Biol, 27, 1504–1517, https://doi.org/10.1111/gcb.15510, 2021.

Brighenti, S., Colombo, N., Wagner, T., Pettauer, M., Guyennon, N., Krainer, K., Tolotti, M., Rogora, M., Paro, L., and Steingruber, S. M.: Factors controlling the water quality of rock glacier springs in European and American mountain ranges, Sci Total Environ, 953, 175706, 2024.

Charbonneau, A. A. and Smith, D. J.: An inventory of rock glaciers in the central british columbia coast mountains, canada, from high resolution google earth imagery, Arct., Antarc., Alp. Res., 50, e1489026, https://doi.org/10.1080/15230430.2018.1489026, 2018.

D. B. Jones, Harrison, S., Anderson, K., and Betts, R. A.: Mountain rock glaciers contain globally significant water stores, Sci Rep, 8, 2834, https://doi.org/10.1038/s41598-018-21244-w, 2018.

Erharter, G. H., Wagner, T., Winkler, G., and Marcher, T.: Machine learning – An approach for consistent rock glacier mapping and inventorying – Example of Austria, Appl Comput Geosci, 16, 100093, https://doi.org/10.1016/j.acags.2022.100093, 2022.

Eriksen, H. Ø., Rouyet, L., Lauknes, T. R., Berthling, I., Isaksen, K., Hindberg, H., Larsen, Y., and Corner, G. D.: Recent Acceleration of a Rock Glacier Complex, Ádjet, Norway, Documented by 62 Years of Remote Sensing Observations, Geophys Res Lett, 45, 8314–8323, https://doi.org/10.1029/2018GL077605, 2018.

Farinotti, D., Huss, M., Fürst, J. J., Landmann, J., Machguth, H., Maussion, F., and Pandit, A.: A consensus estimate for the ice thickness distribution of all glaciers on Earth, Nat. Geosci., 12, 168–173, https://doi.org/10.1038/s41561-019-0300-3, 2019.

Feng, M., Xu, J., Zhang, X., Yan, D., Li, X., Kääb, A., Chen, F., and Cheng, G.: Underestimated number and significance of rock glaciers on the Tibetan Plateau, Sci. Bull., https://doi.org/10.1016/j.scib.2025.12.004, 2025.

French, H. M.: The periglacial environment, John Wiley & Sons, 2017.

Gruber, S.: Derivation and analysis of a high-resolution estimate of global permafrost zonation, Cryosphere, 6, 221–233, https://doi.org/10.5194/tc-6-221-2012, 2012.

https://doi.org/10.5194/essd-2026-575
Preprint. Discussion started: 2 November 2026
© Author(s) 2026. CC BY 4.0 License.



Haeberli, W., Hallet, B., Arenson, L., Elconin, R., Humlum, O., Kääb, A., Kaufmann, V., Ladanyi, B., Matsuoka, N., Springman, S., and Mühll, D. V.: Permafrost creep and rock glacier dynamics, Permafr Periglac Process, 17, 189–214, https://doi.org/10.1002/ppp.561, 2006.

Haeberli, W., Arenson, L. U., Wee, J., Hauck, C., and Mölg, N.: Discriminating viscous-creep features (rock glaciers) in mountain permafrost from debris-covered glaciers – a commented test at the Gruben and Yerba Loca sites, Swiss Alps and Chilean Andes, Cryosphere, 18, 1669–1683, https://doi.org/10.5194/tc-18-1669-2024, 2024.

Harrington, J. S., Mozil, A., Hayashi, M., and Bentley, L. R.: Groundwater flow and storage processes in an inactive rock glacier, Hydrological Processes, 32, 3070–3088, https://doi.org/10.1002/hyp.13248, 2018.

Hartl, L., Fischer, A., Stocker-waldhuber, M., and Abermann, J.: Recent speed-up of an alpine rock glacier: an updated chronology of the kinematics of outer hochebenkar rock glacier based on geodetic measurements, Geografiska Annaler: Series A, Physical Geography, 98, 129–141, https://doi.org/10.1111/geoa.12127, 2016.

Hassan, J., Chen, X., Muhammad, S., and Bazai, N. A.: Rock glacier inventory, permafrost probability distribution modeling and associated hazards in the Hunza River Basin, Western Karakoram, Pakistan, Sci Total Environ, 782, 146833, https://doi.org/10.1016/j.scitotenv.2021.146833, 2021.

Hassan, J., Berg, D. L., Lippert, E. Y. H., Chen, X., Hassan, W., Hassan, M., Hussain, I., Bazai, N. A., and Khan, S. A.: Rock glacier distribution and kinematics in shigar and shayok basins based on radar and optical remote sensing, Earth Surf Process Landf, 49, 2278–2290, https://doi.org/10.1002/esp.5820, 2024.

Hawker, L., Uhe, P., Paulo, L., Sosa, J., Savage, J., Sampson, C., and Neal, J.: A 30 m global map of elevation with forests and buildings removed, Environ. Res. Lett., 17, 024016, https://doi.org/10.1088/1748-9326/ac4d4f, 2022.

Hu, Y., Liu, L., Huang, L., Zhao, L., Wu, T., Wang, X., and Cai, J.: Mapping and characterizing rock glaciers in the arid Western Kunlun Mountains supported by InSAR and deep learning, J Geophys Res Earth Surf, 128, e2023JF007206, https://doi.org/10.1029/2023JF007206, 2023.

Hu, Z., Yan, D., Feng, M., Xu, J., Liang, S., and Sheng, Y.: Enhancing mountainous permafrost mapping by leveraging a rock glacier inventory in northeastern Tibetan Plateau, Int J Digit Earth, 17, 2304077, https://doi.org/10.1080/17538947.2024.2304077, 2024.

IANIGLA: Resumen ejecutivo de los resultados del Inventario Nacional de Glaciares, IANIGLA-CONICET, Ministerio de Ambiente y Desarrollo Sustentable de la Nación,

https://doi.org/10.5194/essd-2026-575
Preprint. Discussion started: 2 November 2026
© Author(s) 2026. CC BY 4.0 License.



2018.

Janke, J. R., Williams, M. W., and Evans, A.: A comparison of permafrost prediction models along a section of Trail Ridge Road, Rocky Mountain National Park, Colorado, USA, Geomorphology, 138, 111–120, https://doi.org/10.1016/j.geomorph.2011.08.029, 2012.

Johnson, G., Chang, H., and Fountain, A.: Active rock glaciers of the contiguous United States: geographic information system inventory and spatial distribution patterns, Earth Syst Sci Data, 13, 3979–3994, https://doi.org/10.5194/essd-13-3979-2021, 2021.

Kääb, A., Strozzi, T., Bolch, T., Caduff, R., Trefall, H., Stoffel, M., and Kokarev, A.: Inventory and changes of rock glacier creep speeds in ile alatau and kungöy ala-too, northern tien shan, since the 1950s, Cryosphere, 15, 927–949, https://doi.org/10.5194/tc-15-927-2021, 2021.

Karger, D. N., Conrad, O., Böhner, J., Kawohl, T., Kreft, H., Soria-Auza, R. W., Zimmermann, N. E., Linder, H. P., and Kessler, M.: Climatologies at high resolution for the Earth's land surface areas, Sci. Data, 4, 170122, https://doi.org/10.1038/sdata.2017.122, 2017.

Kellerer-Pirklbauer, A., Lieb, G. K., and Kleinferchner, H.: A new rock glacier inventory of the Eastern European Alps, Austrian J Earth Sci, 105, 78–93, 2012.

Knight, J.: A new model of rock glacier dynamics, Geomorphology, 340, 153–159, https://doi.org/10.1016/j.geomorph.2019.05.008, 2019.

Kofler, C., Steger, S., Mair, V., Zebisch, M., Comiti, F., and Schneiderbauer, S.: An inventory-driven rock glacier status model (intact vs. relict) for South Tyrol, Eastern Italian Alps, Geomorphology, 350, 106887, https://doi.org/10.1016/j.geomorph.2019.106887, 2020.

Kofler, C., Mair, V., Gruber, S., Todisco, M. C., Nettleton, I., Steger, S., Zebisch, M., Schneiderbauer, S., and Comiti, F.: When do rock glacier fronts fail? Insights from two case studies in South Tyrol (Italian Alps), Earth Surf Process Landf, 46, 1311–1327, https://doi.org/10.1002/esp.5099, 2021.

Körner, C., Jetz, W., Paulsen, J., Payne, D., Rudmann-Maurer, K., and Spehn, E. M.: A global inventory of mountains for bio-geographical applications, Alp. Bot., 127, 1–15, https://doi.org/10.1007/s00035-016-0182-6, 2017.

Krainer, K. and Ribis, M.: A rock glacier inventory of the Tyrolean Alps (Austria), Austrian J Earth Sci, 105, 32–47, 2012.

Lambiel, C. and Delaloye, R.: Contribution of real-time kinematic GPS in the study of

https://doi.org/10.5194/essd-2026-575
Preprint. Discussion started: 2 November 2026
© Author(s) 2026. CC BY 4.0 License.



creeping mountain permafrost: examples from the western swiss alps, Permafrost Periglacial Processes, 15, 229–241, https://doi.org/10.1002/ppp.496, 2004.

Li, X.: Academician guodong cheng's contributions to permafrost science, Permafrost Periglacial Processes, 35, 395–411, https://doi.org/10.1002/ppp.2225, 2024.

Lugon, R. and Stoffel, M.: Rock-glacier dynamics and magnitude–frequency relations of debris flows in a high-elevation watershed: Ritigraben, Swiss Alps, Glob Planet Change, 73, 202–210, https://doi.org/10.1016/j.gloplacha.2010.06.004, 2010.

Lytkin, V.: Inventory and distribution of rock glaciers in northeastern Yakutia, Land, 9, 384, https://doi.org/10.3390/land9100384, 2020.

Manchado, A. M.-T., Allen, S., Cicoira, A., Wiesmann, S., Haller, R., and Stoffel, M.: 100 years of monitoring in the Swiss National Park reveals overall decreasing rock glacier velocities, Commun Earth Environ, 5, 138, https://doi.org/10.1038/s43247-024-01302-0, 2024.

Martini, J., Brighenti, S., Vanek, M., Schwingshackl, T., Vallefuoco, F., Scotti, A., Lencioni, V., and Bottarin, R.: Rock glacier springs: cool habitats for species on the edge, Biodivers Conserv, 33, 4017–4042, https://doi.org/10.1007/s10531-024-02937-3, 2024.

Medina, K., León, H., Badillo-Rivera, E., Loarte, E., Bodín, X., and Úbeda, J.: A comprehensive rock glacier inventory for the Peruvian Andes (PRoGI): dataset, characterization and topoclimatic attributes, Earth Syst Sci Data, 18, 345–369, https://doi.org/10.5194/essd-18-345-2026, 2026.

Millar, C. I. and Westfall, R. D.: Geographic, hydrological, and climatic significance of rock glaciers in the Great Basin, USA, Arctic, Antarctic, and Alpine Research, 51, 232–249, https://doi.org/10.1080/15230430.2019.1618666, 2019.

NASA JPL: NASADEM merged DEM global 1 arc second (V001), https://doi.org/10.5067/MEASURES/NASADEM/NASADEM_HGT.001, 2020.

Obu, J., Westermann, S., Kääb, A., and Bartsch, A.: Ground temperature map, 2000-2016, northern hemisphere permafrost, https://doi.org/10.1594/PANGAEA.888600, 2018.

Obu, J., Westermann, S., Kääb, A., and Bartsch, A.: Ground temperature map, 2000-2016, andes, new zealand and east african plateau permafrost, https://doi.org/10.1594/PANGAEA.905512, 2019a.

Obu, J., Westermann, S., Kääb, A., and Bartsch, A.: Ground temperature map, 2000-2017, antarctic, https://doi.org/10.1594/PANGAEA.902576, 2019b.

https://doi.org/10.5194/essd-2026-575
Preprint. Discussion started: 2 November 2026
© Author(s) 2026. CC BY 4.0 License.



Onaca, A., Ardelean, F., Urdea, P., and Magori, B.: Southern carpathian rock glaciers: inventory, distribution and environmental controlling factors, Geomorphology, 293, 391–404, https://doi.org/10.1016/j.geomorph.2016.03.032, 2017.

Pfeffer, W. T., Arendt, A. A., Bliss, A., Bolch, T., Cogley, J. G., Gardner, A. S., Hagen, J.-O., Hock, R., Kaser, G., Kienholz, C., Miles, E. S., Moholdt, G., Mölg, N., Paul, F., Radić, V., Rastner, P., Raup, B. H., Rich, J., Sharp, M. J., and Consortium, T. R.: The Randolph Glacier Inventory: a globally complete inventory of glaciers, J Glaciol, 60, 537–552, https://doi.org/10.3189/2014JoG13J176, 2014.

Ran, Z. and Liu, G.: Rock glaciers in daxue shan, south-eastern Tibetan Plateau: an inventory, their distribution, and their environmental controls, Cryosphere, 12, 2327–2340, https://doi.org/10.5194/tc-12-2327-2018, 2018.

Rangecroft, S., Harrison, S., and Anderson, K.: Rock glaciers as water stores in the Bolivian Andes: An assessment of their hydrological importance, Arct Antarct Alp Res, 47, 89–98, https://doi.org/10.1657/AAAR0014-029, 2015.

Remya, S. N., Ghosh, T., Agarwal, V., Majeed, Z., Govindha Raj K, B., Sharma, A., Kulkarni, A. V., Ahmad Mukhtar, M., and Mishra, R.: A framework to identify rock glaciers and model mountain permafrost in the Jhelum Basin, Kashmir Himalaya, India, Earth and Space Science, 11, e2023EA003170, https://doi.org/10.1029/2023EA003170, 2024.

RGIK: Guidelines for inventorying rock glaciers: Baseline and practical concepts (Version 1.0), https://doi.org/10.51363/unifr.srr.2023.002, 2023.

Roer, I., Haeberli, W., Avian, M., Kaufmann, V., Delaloye, R., Lambiel, C., and Kääb, A.: Observations and considerations on destabilizing active rock glaciers in the European Alps, Ninth International Conference on Permafrost, 1505–1510, https://doi.org/10.5167/uzh-6082, 2008.

Rouyet, L., Lilleøren, K. S., Böhme, M., Vick, L. M., Delaloye, R., Etzelmüller, B., Lauknes, T. R., Larsen, Y., and Blikra, L. H.: Regional morpho-kinematic inventory of slope movements in northern Norway, Front. Earth Sci., 9, https://doi.org/10.3389/feart.2021.681088, 2021.

Rouyet, L., Bolch, T., Brardinoni, F., Caduff, R., Cusicanqui, D., Darrow, M., Delaloye, R., Echelard, T., Lambiel, C., Pellet, C., Ruiz, L., Schmid, L., Sirbu, F., and Strozzi, T.: Rock Glacier Inventories (RoGIs) in 12 areas worldwide using a multi-operator consensus-based procedure, Earth Syst Sci Data, 17, 4125–4157, https://doi.org/10.5194/essd-17-4125-2025, 2025.

Schaffer, N., MacDonell, S., Réveillet, M., Yáñez, E., and Valois, R.: Rock glaciers as a water resource in a changing climate in the semiarid Chilean Andes, Reg Environ

https://doi.org/10.5194/essd-2026-575
Preprint. Discussion started: 2 November 2026
© Author(s) 2026. CC BY 4.0 License.



Change, 19, 1263–1279, https://doi.org/10.1007/s10113-018-01459-3, 2019.

Sun, Z., Hu, Y., Racoviteanu, A., Liu, L., Harrison, S., Wang, X., Cai, J., Guo, X., He, Y., and Yuan, H.: TPRoGI: a comprehensive rock glacier inventory for the Tibetan Plateau using deep learning, Earth Syst Sci Data, 16, 5703–5721, https://doi.org/10.5194/essd-16-5703-2024, 2024.

Tielidze, L. G., Cicoira, A., Nosenko, G. A., and Eaves, S. R.: The first rock glacier inventory for the Greater Caucasus, Geosciences, 13, 117, https://doi.org/10.3390/geosciences13040117, 2023.

Wagner, T., Seelig, S., Helfricht, K., Fischer, A., Avian, M., Krainer, K., and Winkler, G.: Assessment of liquid and solid water storage in rock glaciers versus glacier ice in the Austrian Alps, Sci Total Environ, 800, 149593, https://doi.org/10.1016/j.scitotenv.2021.149593, 2021.

Wang, X., Liu, L., Zhao, L., Wu, T., Li, Z., and Liu, G.: Mapping and inventorying active rock glaciers in the northern Tien Shan of China using satellite SAR interferometry, Cryosphere, 11, 997–1014, https://doi.org/10.5194/tc-11-997-2017, 2017.

Wilson, E. B.: Probable inference, the law of succession, and statistical inference, J. Am. Stat. Assoc., 22, 209–212, https://doi.org/10.1080/01621459.1927.10502953, 1927.

Xu, J., Feng, M., Su, Y., Yan, D., Wu, Q., Zhao, P., Zhang, X., and Li, X.: A global rock glacier inventory dataset. National Tibetan Plateau / Third Pole Environment Data Center, https://doi.org/10.11888/Cryos.tpdc.303562, 2026.

Yan, D., Feng, M., Hu, Z., Xu, J., and Li, X.: Improving permafrost mapping in southern Tibetan Plateau using machine learning and rock glacier inventory, Permafr Periglac Process, 36, 230–244, https://doi.org/10.1002/ppp.2266, 2025.

Zemp, M., Chao, Q., Han Dolman, A. J., Herold, M., Krug, T., Speich, S., Suda, K., Thorne, P., and Yu, W.: GCOS 2022 implementation plan, World Meteorological Organization, Geneva, Switzerland, 2022.

Zhang, X., Feng, M., Zhang, H., Wang, C., Tang, Y., Xu, J., Yan, D., and Wang, C.: Detecting rock glacier displacement in the central Himalayas using multi-temporal InSAR, Remote Sens, 13, 4738, https://doi.org/10.3390/rs13234738, 2021.